Title: *DNA methylation profiling in pheochromocytoma and paraganglioma reveals diagnostic and prognostic markers.*

Authors:

Aguirre A. de Cubas[1], Esther Korpershoek[2], Lucia Inglada-Pérez[1,3], Eric Letouzé[4], Maria Currás-Freixes[1], Agustin F. Fernández[5], Iñaki Comino-Méndez[1], Francesca Schiavi[6], Veronika Mancikova[1], Graeme Eisenhofer[7,8], Massimo Mannelli[9], Guiseppe Opocher[6,10], Henri Timmers[11], Felix Beuschlein[12], Ronald de Krijger[13], Alberto Cascon[1,3], Cristina Rodríguez-Antona[1,3], Mario F. Fraga[5,14], Judith Favier[15,16,*], Anne-Paule Gimenez-Roqueplo[15,16,17,18*], and Mercedes Robledo[1,3,†].

Affiliations:

1. Hereditary Endocrine Cancer Group, Spanish National Cancer Research Centre (CNIO), Madrid, Spain.
2. Department of Pathology, Erasmus MC Cancer Institute, University Medical Center, Rotterdam, The Netherlands.
3. Centro de Investigación Biomédica en Red de Enfermedades Raras (CIBERER), Madrid, Spain.
4. Programme Cartes d'Identité des Tumeurs, Ligue Nationale Contre Le Cancer, 75013 Paris, France.
5. Cancer Epigenetics Laboratory, Institute of Oncology of Asturias (IUOPA), HUCA, University of Oviedo, Asturias, Spain.
6. Familial Cancer Clinic, Veneto Institute of Oncology, Padova, Italy.
7. Institute of Clinical Chemistry and Laboratory Medicine, Technische Universität Dresden, Dresden, Germany.
8. Medical Clinic III, Technische Universität Dresden, Dresden, Germany.
9. Department of Experimental and Clinical Biomedical Sciences, University of Florence, Florence, Italy.
10. Department of Medicine, University of Padova, Padova, Italy.
11. Internal Medicine, Radboud University Medical Centre, Nijmegen, The Netherlands.
12. Department of Internal Medicine IV Campus Innenstadt, University-Hospital, Ludwig-Maximilians-University of Munich, D-81377 Munich, Germany.
13. Department of Pathology, Josephine Nefkens Institute, Erasmus MC University Medical Center, Rotterdam, The Netherlands.
14. Department of Immunology & Oncology, National Center for Biotechnology, CNB-CSIC, Cantoblanco, Madrid, Spain.
15. INSERM, UMR970, Paris-Cardiovascular Research Center (PARCC), 75015 Paris, France.
16. Faculté de Médecine, Université Paris Descartes, Sorbonne Paris Cité, 75006 Paris, France.
17. Service de Génétique, Assistance Publique Hôpitaux de Paris, Hôpital européen Georges Pompidou, 75015 Paris
18. Rare Adrenal Cancer Network-Cortico Médullosurrénale Tumeur Endocrine, Institut National du Cancer, 75014 Paris, France.
*These authors contributed equally to the article

Running title: DNA methylation profiling in PPGL. Novel prognostic markers.

Keywords (5)

1. Metastatic pheochromocytoma
2. Paraganglioma
3. DNA methylation
4. Prognosis
5. Hypermethylation

Funding

This work was supported by ENS@T-Cancer – the work leading to these results has received funding from the European Union Seventh Framework Programme (FP7/2007-2013) under grant agreement no. 259735. Also, in part by the fundacion Mutua Madrileña (project AP2775/2008) and the Fondo de Investigaciones Sanitarias (projects PI11/01359 and PI14/00240). AAdeC and VM are predoctoral fellows of The "Caixa"/CNIO international PhD programme. LI-P is supported by the CIBERER.

Corresponding author

†Address correspondence to: Mercedes Robledo

Hereditary Endocrine Cancer Group, Human Cancer Genetics Programme. Centro

Nacional de Investigaciones Oncológicas, CNIO)

Melchor Fernández Almagro 3, 28029 Madrid, Spain

Phone: +34-91-224 69 47 | Fax: +34-91-224 69 23

E-mail: mrobledo@cnio.es

Conflict of Interest

The authors declare that there is no conflict of interest that could be perceived as prejudicing the impartiality of the research reported.

Abstract word Count: 250

Manuscript word Count: 5000

Total Figures: 2

Total Tables: 3

Total Supplemental Tables: 2

Total Supplemental Figures: 1

TRANSLATIONAL RELEVANCE

Pheochromocytoma and paraganglioma (PPGL) are rare tumors that often present highly variable, post-operative outcomes. Current therapeutic options for metastatic PPGL are very limited. Therefore, novel prognostic markers for metastatic PPGL are urgently needed. In this study, we investigated, identified and validated novel prognostic and predictive markers for PPGLs presenting metastases using whole-genome DNA methylation profiling data from two large, well-characterized discovery and primary validation series of tumors. Even after correcting for *SDHB* genotype, 48 of these CpGs showed significant associations with time to progression, indicating potential utility as novel molecular predictive markers. Our findings suggested that aberrant DNA methylation might affect nervous system development and transcriptional regulation networks in PPGL with metastases, providing potential clues for future therapeutic strategies. Specifically, these analyses indicated *RDBP* hypermethylation in metastatic tumors, which we validated in another second independent series, disrupted the expression of various key molecules that we also observed in transcriptomic analyses.

ABSTRACT

Purpose:

Pheochromocytoma and paraganglioma (PPGL) are rare neuroendocrine tumors, associated with highly variable post-operative evolution. The scarcity of reliable PPGL prognostic markers continues to complicate patient management. In this study, we explored genome-wide DNA methylation patterns in the context of PPGL malignancy to identify novel prognostic markers.

Experimental Design:

We retrospectively investigated DNA methylation patterns in PPGL with and without metastases utilizing high-throughput DNA methylation profiling data (Illumina 27K) from two large, well-characterized discovery (n=123; 24 metastatic) and primary validation (n=154; 24 metastatic) series. Additional validation of candidate CpGs was performed by bisulfite pyrosequencing in a second independent set of 33 paraffin-embedded PPGLs (19 metastatic).

Results:

Of the initial 86 candidate CpGs, we successfully replicated fifty-two (47 genes), associated with metastatic PPGL. Of these, 48 CpGs showed significant associations with time to progression even after correcting for SDHB genotype, suggesting their value as prognostic markers independent of genetic background. Hypermethylation of *RDBP* (negative elongation factor complex member E) in metastatic tumors was further validated by bisulfite pyrosequencing ($\Delta\beta_{\text{metastatic-benign}}$=0.29, p=0.003; HR: 1.4 (CI95%: 1.1-2.0), p=0.018), and may alter transcriptional networks involving (*RERG*, *GPX3*, and *PDZK1*) apoptosis, invasion, and maintenance of DNA integrity.

Conclusion:

This is the first large-scale study of DNA methylation in metastatic PPGL that identifies and validates prognostic markers, which could be used for stratifying patients according to risk of developing metastasis. Of the three CpGs selected for further validation, one (*RDBP*) was clearly confirmed, and could be used for stratifying patients according to the risk of developing metastases.

INTRODUCTION

Pheochromocytoma and paraganglioma (PPGL) are rare neuroendocrine tumors that arise from the adrenal medulla and paraganglial system, respectively. PPGLs can arise as part of hereditary syndromes associated with germline mutations in at least fifteen genes and has been extensively discussed elsewhere (1, 2). Extensive clinical and genetic characterization over the last 25 years has greatly improved our knowledge about the genetic basis underlying PPGLs. Fortunately, application of high-throughput technologies to study PPGL have enhanced our understanding of tumor biology and has already led to novel therapeutic strategies, which may soon be applied in routine clinical practice (3-7). However, lack reliable markers for metastatic disease and/or their limited predictive value continue to complicate the clinical management of PPGL patients. Therefore, identifying and validating novel prognostic/predictive markers for high-risk PPGL patients is of paramount importance for appropriate patient management and also help guide therapeutic strategies (5, 7).

Previous cytogenetic, transcriptomic and miRNA expression performed in PPGL have shed light on some of the molecular events underlying these tumors (3, 4). Notwithstanding, the epigenetic landscape in PPGL has just only recently been explored (2, 8). DNA methylation is a well-known regulatory mechanism involved in normal development and in disease pathogenesis, including cancer. In human neoplasms, hypomethylated genomic DNA was found to promote genomic instability, while hypermethylated genomic regions frequently mediate the silencing of tumor suppressor genes (TSGs) (9). Consequently, DNA methylation has become the most widely studied epigenetic modification, and promise as novel disease-specific and/or prognostic markers.

Previously, epigenetic studies in PPGL followed candidate gene approaches. In addition to being limited to small sets of CpGs, these early studies were biased toward hypermethylation of known genes, usually TSGs (10, 11). It was not until recently that whole genome DNA methylation profiles were explored in PPGLs (2). Consistent with previous high-throughput studies, DNA methylation in PPGLs was found to be highly dependent on genetic background. Global DNA hypermethylation was described as a hallmark of tumors with Krebs cycle abnormalities resulting from *SDHx* and *FH* mutations (2). Although genetic background was found to strongly influence DNA methylation patterns in PPGL, these epigenetic aberrations have yet to be comprehensively explored in metastatic PPGL.

In this study, we explored DNA methylation patterns in metastatic PPGL using two large, well-characterized cohorts of PPGL collected through a multi-institutional collaboration within the European Network for the Study of Adrenal Tumors (ENS@T). Candidate CpGs associated with metastatic PPGL were identified using whole genome DNA methylation profiles obtained from a discovery series containing 24 metastatic (4 *SDHB*) PPGLs. These data were replicated for fifty-two of these candidate CpGs in a first validation series, which comprised whole genome DNA methylation data (27K Illumina) containing 154 PPGL, including 24 metastatic tumors (10 *SDHB*). Interestingly, significant associations with time to progression (TTP) were found for a large proportion of these CpGs. Among these CpGs, hypermethylation of the *RDBP* (negative elongation factor complex member E) gene in metastatic PPGLs was further validated in a third series by bisulfite pyrosequencing ($\Delta\beta_{metastatic\text{-}benign}$=0.29, p=0.003; HR: 1.4, CI95%: 1.1-2.0, p=0.018) of 33 formalin fixed paraffin-embedded (FFPE) tissues. Bioinformatics analyses suggested *RDBP* hypermethylation might contribute to metastatic disease by altering transcriptional networks, including those involved in response to apoptotic stimuli, invasion, and maintenance of DNA integrity. Our results suggest that these CpGs may represent potential markers of malignancy and also serve as prognostic predictors independent of genetic background.

MATERIALS AND METHODS

Patient Samples

According to standard protocols, all patients underwent tumor resective surgery four to six weeks after diagnosis of PPGL. All fresh-frozen tissues were immediately frozen in liquid nitrogen and stored at -80°C. PPGL was confirmed by pathologic examination. All samples included in this study contained at least 85% tumor cells. A PPGL was considered metastatic when the patient presented metastases at non-chromaffin sites distant from the primary tumor (Supplemental Table 1).

For this retrospective study, a total of 310 tumors were obtained from patients with confirmed PPGL diagnosis, recruited through collaborating centers of the European Network for the Study of Adrenal Tumors (ENS@T) according to the Reporting Recommendations for Tumor Marker prognostic Studies (REMARK) guidelines (12). Discovery series (n=123) and validation series 2 (n=33) samples were collected from 1989 to 2012 through seven institutions: Spanish National Cancer Research Centre (Madrid, Spain); Erasmus MC Cancer Institute (Rotterdam, The Netherlands); Ludwig-Maximilians-University of Munich (Munich, Germany); Radboud University Medical Centre (Nijmegen, The Netherlands); Veneto Institute of Oncology (Padua, Italy); Technische Universität Dresden (Dresden, Germany); and University of Florence (Florence, Italy). Validation series 1 samples (n=154) were collected from patients recruited through the COMETE (Cortico et Médullosurrénale: les Tumeurs Endocrines) network from 1993 to 2008 (2). All patients provided written informed consent for the collection of samples and subsequent analyzes. Ethical approval for the study was obtained from each institutional review board from all collaborating centers.

Median age and gender ratio (female:male) were 44 years and 1.28, respectively. There were no statistically significant differences among median age distribution and gender ratio between series (Mann-Whitney's U associated p-values>0.05). These 310 tumors represent three series: discovery series (DS), and validation series (VS1 and VS2). The DS was composed of 123 fresh-frozen PPGL specimens (24 metastatic). Genetic screening for DS samples was performed as previously described (3, 13, 14). The 99 PPGLs without metastasis contained 22 *VHL*, 26 *RET*, 8 *NF1*, 4 *SDHB*, 2 *SDHD*, 4 *EPAS1*, 2 *MAX*, 2 *HRAS*, and 1 *TMEM127* mutations, and 28 tumors ("wild-type" or WT) had no mutations in known susceptibility genes. The 24 metastatic tumors were mostly WT (n=17) with the rest being 4 *SDHB*-, 2 *MAX*-, and 1 *VHL*-related PPGLs.

DNA methylation data from another large cohort (VS1) of PPGLs was obtained from Gene Expression Omnibus (GEO, www.ncbi.nlm.nih.gov/gds), under accession number GSE39198 (2). VS1 was expanded with ten additional metastatic specimens (previously unpublished), also provided by the COMETE network. VS1 contained a total of 154 PPGLs. Of these, 24 were metastatic tumors and included 10 *SDHB*-, 5 *VHL*-, 2 *NF1*-, and 1 *FH*-related PPGLs, as well as six WT tumors. VS1 samples were collected prospectively by the COMETE network, and genetic screening was performed as previously described (2). Ethical approval for the study was obtained from the local institutional review board [Comité de Protection des Personnes (CPP) Ile de France III, June 2012]. Written informed consent for the sample collection and subsequent analyses was obtained from all patients (2).

For further validation, we compiled an additional independent series (VS2) of FFPE PPGLs (n=33; 19 metastatic) through ENS@T. Like DS and VS1 cohorts, VS2 was composed of only pheochromocytomas and sympathetic paragangliomas, and contained no parasympathetic paragangliomas. Of these thirty-three PPGLs, 19 were metastatic (16 WT, 1 *SDHA*, 1 *HRAS*, and 1 *VHL*) and 14 samples were non-metastatic (3 *SDHB*, 2 *VHL*, 1 *HRAS*, and 8 WT). Tumors from Erasmus MC University Medical Center were assessed anonymously according to the Proper Secondary Use of Human Tissue code established by the Dutch Federation of Medical Scientific Societies (http:// www.federa.org).

A summary of clinical features for DS, VS1, and VS2 PPGLs is shown in Table 1 (more detailed clinical information is provided in Supplemental Table 1).

DNA extraction and purification and DNA methylation assay

As for VS1 samples, DNA from DS and VS2 samples was extracted and purified using the DNeasy Blood and Tissue Kit (Qiagen, Chatsworth, CA, USA) according to the manufacture's protocol (2).

Bisulfite-conversion of DNA was performed using the EZ DNA Methylation Kit (Zymo Research, Orange, CA) following the manufacturer's recommendations. Genome-wide DNA methylation was assayed using the Illumina Infinium HumanMethylation 27K Platform (Illumina, San Diego, CA) at the Spanish, "Centro Nacional de Genotipado (CEGEN-ISCIII)" (www.cegen.org), as previously described (15).

Data processing

The Illumina 27K array interrogates 27,578 CpGs. Beta-values for each interrogated CpG were assigned using the Genome Studio Methylation module. To correct for the heteroskedasticity observed for beta-values, Beta-values were transformed to M-values, defined as log2 (methylated probe intensity/unmethylated probe intensity). Negative M-values indicate less than 50% methylation and positive M-values indicate more than 50% methylation (16). Thus, M-values were used for all statistical analysis (supervised and TTP analyses), while beta-values were used for biological interpretation (e.g. difference in methylation) (16).

Data analysis and statistical methods

All unsupervised and supervised analyses were performed using "R". The top 500 probes with the highest variance across all samples were used for unsupervised analysis. The "ConsensusClusterPlus" package was used for consensus cluster analysis (17).

For all statistical analyses performed involving multiple testing, p-values were adjusted accordingly by the Benjamini & Hochberg method (q-values) (18). All supervised analyses were performed using the "limma" package, and were limited to experimental groups with at least three samples. All samples in DS (n=123) and VS1 (n=154) (Supplemental Table 1) were included in supervised analyses. Only significantly methylated CpGs (q-value <0.10 and $\Delta\beta > |0.2|$) were considered for subsequent analyses. Comparisons between the different PPGL genetic groups were performed always relative to the *SDHB* group to facilitate inter-group comparisons.

First, candidate CpGs associated with metastatic PPGL were identified by supervised analysis comparing DS samples with and without metastasis (q-value <0.10 and $\Delta\beta > |0.2|$). Candidate CpGs were further distilled filtering out those probes not present in at least 50% of metastatic PPGLs. To refine selection of candidate CpGs, DNA methylation patterns of candidate CpGs were assessed in VS1. Only those successfully replicated CpGs were considered for further analyses. *SDHB* PPGLs have recently shown to have a CpG island hypermethylator phenotype (high-CIMP) with a previously defined signature of 298 hypermethylated CpGs (2). Thus, we further filtered the data for these probes. Those CpGs meeting all the above criteria were considered as candidate CpG markers associated with metastatic PPGL.

To determine the potential impact of DNA methylation at candidate CpGs TTP, we performed a Cox regression for individual CpG data as continuous variables (as M-values).

TTP was defined as the time between the date of surgery to date of first documented detection of metastases (metastases delay). Patients without documented evidence of metastases were censored at the date of last follow-up. Only samples from patients presenting metachronous metastases were included in survival analyses, while samples from patients with synchronous metastases, defined as those presenting at diagnosis or surgery (event time=0), were excluded from these analyses. As DS and VS1 data were generated with the same platform, we pooled samples to form a larger collection of tumors to permit TTP analyses. After filtering-out samples from patients with synchronous metastases (n=25), as well as those samples without complete follow-up (n=19), there remained 233 tumors including 23 metastatic PPGLs (events). The final model was adjusted for *SDHB* mutation, series origin of tumors, and multiple testing as described above (18). For Kaplan-Meier plots, methylation M-values were converted to binary variables using the median as the cutoff value. These variables were defined as 0 (hypomethylated) for those valued less than the median cutoff, while values greater than the cutoff were considered as 1 (hypermethylated). The association between methylation at individual CpGs and TTP was estimated using the method of Kaplan and Meier and assessed using the log-rank test. Kaplan-Meier curves and analyses were performed using SPSS version 17 (SPSS inc., Chicago, IL).

Venn diagram analyses were performed with the "Vennerable" package (http://vennerable.sourceforge.net/), and circos plots were generated using the "circlize" and "RCircos" package. Pathway analysis was performed using the PantherDB classification system (http://www.pantherdb.org/) and DAVID Bioinformatics Resources 6.7 (http://david.abcc.ncifcrf.gov/home.jsp).

Bisulfite pyrosequencing

Among those candidate CpGs associated with metastatic PPGL, three were selected for further validation by bisulfite pyrosequencing in VS2 (33 FFPE PPGLs). These CpGs were selected because they showed highly different methylation levels and because of the reported biological functions of the corresponding genes.

Bisulfite modification of DNA was performed as described above. Primers for PCR amplification and sequencing were designed with PyroMark assay design (version 2.0.01.15) software. Primer sequences were designed to hybridize with CpG free sites to ensure methylation-independent amplification (Supplemental Table 2). PCRs were performed with biotinylated primers to convert the PCR product to single-stranded DNA templates with the Vacuum Prep Tool. After PCR amplification, pyrosequencing reactions

and methylation quantification were performed using PyroMark Q24 reagents, equipment and software according to manufacturer's instructions (Qiagen). Quantitation of DNA methylation for a given CpG by bisulfite pyrosequencing is given as the percentage of 5-methylcytosine representative of the C-to-T ratio (100xβvalue). Significance was assessed by Student T-Test. TTP was calculated in FFPE samples by Cox regression for *RDBP* as continuous variables (M-values), as described above.

GEO Datasets

Gene expression profiling data for 99 PPGLs, containing 8 with and 91 without metastasis, was obtained through gene expression omnibus (GEO) under GSE19422 and GSE51087. Gene expression profiling data for T47D breast cancer cells with and without *RDBP* knock out was accessed through GEO (GSE19940). As previously described, downloaded gene expression profiles were quantile normalized and antigenomic probes were used as background probes (3, 19, 20).

RESULTS

DNA methylation profiling in DS and VS1

DNA methylation data for DS tumors was deposited on gene expression omnibus under the GEO accession number GSE62231, and the ten additional metastatic PPGLs of the VS1 tumors from the COMETE network under the accession number GSE43298. Probes on the X or Y chromosome (n=1085 or n=7, respectively), as well as unreliable probes not detected with p>0.01 in more than 5% of samples (n=1029), were removed. The remaining 25,457 probes were used for subsequent analyses. After preprocessing, we obtained β- and M-values of these CpGs for DS PPGLs.

Unsupervised and supervised analyses of PPGL DNA methylation Profiles

Unsupervised hierarchical cluster analysis in DS, split samples into two main clusters, C1 and C2 (Figure 1A). C1, enriched with *VHL*- and *SDHx*-related tumors, was subdivided into 2 subclusters (C1A and C1B). C1A contained seven of eight *SDHB*- and all *SDHD*-related, and 5 WT PPGLs. In total, C1A was composed of 15 tumors, 6 were metastatic. C1B contained 22 *VHL*-, 1 *SDHB*-, 6 *RET*-, 3 *NF1*-, and 3 *EPAS1*-related, and 11 WT tumors. C1B contained 37 PPGLs, 9 with metastases. In addition to 20 *RET*-related tumors, C2 contained 5 *NF1*-, 2 *HRAS*-, 1 *TMEM127*-, 1 *VHL*-, and 1 *EPAS1*-related PPGLs and 28 WT specimens. Nine of 62 tumors in C2 were metastatic.

K-means consensus clustering was performed to verify hierarchical cluster analysis. According to this analysis, the optimal classification defined 3 subgroups, shown in Figure 1B. Cluster memberships for hierarchical cluster and consensus cluster analyses results were highly similar with a 93% (114/123) agreement between the two. Cluster memberships for DS are provided in Supplemental Table 1.

We generated a circus plot (Figure 1C) depicting methylation levels for six genetic classes (*SDHB*, *VHL*, *EPAS1*, *RET*, *NF1*, and *MAX*). Figures 1C-D show varying degrees of methylation among the six groups. *SDHB*-related tumors had highest levels of DNA methylation. *VHL*- and *EPAS1*-related PPGLs showed intermediate levels, while *RET*-, *NF1*-, and *MAX*-related tumors had the lowest levels of DNA methylation. The difference between genotypes was significant (ANOVA; P=0.001). These results verify that *SDHB*-related tumors display a CpG island methylator phenotype (high-CIMP).

Initial comparisons between the different genetic groups and *SDHB*-related tumors in DS identified numerous hypermethylated and hypomethylated CpGs (Table 2). To validate the

above DNA methylation patterns associated with each genetic background, the same analyses were performed in VS1. These analyses were performed for *VHL*-, *RET*-, *NF1*-, *MAX*-, and *SDHB*-associated tumors in VS1, but not for *EPAS1*-related samples, as none were available in VS1 (Table 2). To further determine genotype specific CpGs, as well as those common among all genotypes, we performed Venn diagram analysis with these confirmed probes (Figure 1E). As expected, CpGs in *SDHB*-related tumors were almost all hypermethylated, while the other experimental groups showed a higher proportion of hypomethylated CpGs.

We performed pathway analysis using differentially methylated genes for each inter-group comparisons of PPGLs. Comparisons versus *SDHB*-associated PPGLs showed enrichment in pathways implicated in tumorigenesis, such as "pathways in cancer", "MAPK signaling pathway", "p53 signaling pathways", "ECM-receptor interaction", "focal adhesion", and "apoptosis". Well-known TSGs and mediators of apoptosis were among the hypermethylated genes in *SDHB*-related tumors (Figure 1C). The most over-represented pathways among *VHL*-, *RET*-, *NF1*-, and *MAX*-related tumors relative to *SDHB*-associated PPGLs was "WNT signaling" pathway, followed by "cadherin signaling", "angiogenesis", "integrin signaling", and "adrenaline and noradrenaline biosynthesis" pathways. Among the genes in the “adrenaline and noradrenaline biosynthesis and signaling” pathway (Figure 1C), differential methylation of *PNMT* (phenylethanolamine N-methyltransferase) and *NET* (norepinephrine transporter, *SLC6A2*) was particularly interesting. *PNMT* was hypermethylated in *SDHB*-related PPGLs, intermediately methylated in *VHL*-related tumors, and hypomethylated in *RET*-, *NF1*-, *MAX*-, and *HRAS*-associated PPGLs (Supplemental Figure 1). Also of interest was *MEG3* (maternally expressed gene 3) hypermethylation in *MAX*-related PPGLs.

CpGs associated with metastatic disease and progression

Initial selection of CpG candidates from DS PPGLs (n=123, 24 metastatic), identified 86 differentially methylated probes (q-value<0.10, $\Delta\beta>|0.2|$, and present in at least 50% of metastatic tumors). Fifty-two CpGs (Table 3) were successfully replicated in VS1 (n=154, 24 metastatic). As shown in heatmaps in Figure 2A, there was a high degree of concordance in methylation levels for these 52 CpGs (corresponding to 47 genes) between those tumors with and without metastases in DS and VS1. As we were interested in finding CpGs associated with metastatic PPGLs independent of genetic background, we verified that the above probes were not included among those reported by Letouzé and colleagues in association with *SDHB*-related tumors (2).

TTP analyses were performed using 233 tumors of which 23 were metastatic. These 233 samples had a median follow-up time of 43 months. Forty-eight of 52 CpGs described above showed significant associations with TTP (q-value<0.1) even after adjusting for presence of *SDHB* mutations, series origin, and multiple testing (Table 3).

Pathway analysis performed with genes corresponding to these 52 CpGs indicated biological processes involving "regulation of transcription from RNA polymerase II promoter" and "nervous system development" were potentially affected (Figure 2A).

Validation CpGs by Pyrosequencing

To further confirm our results, we selected three CpGs associated with metastatic PPGL for validation in an independent series of FFPE PPGLs (VS2), containing 19 metastatic tumors. These CpGs corresponded to the following genes: *RDBP, HDAC11* (histone deacetylase 11), and *CYFIP2* (cytoplasmic FMR1 interacting protein 2). As mentioned above, these CpGs also showed highly significant associations with TTP (Figure 2B-D). Of these CpGs, hypermethylation of *RDBP* in metastatic PPGL was validated in VS2, ($\Delta\beta_{metastatic\text{-}benign}$=0.29, p=0.003). The association between *RDBP* methylation and TTP was also confirmed in VS2 (HR: 1.4, CI95%: 1.1-2.0; p=0.018).

Gene expression profiling of *RDBP* knockout

To identify potential RDBP target genes, we downloaded gene expression data for T47D breast cancer cells with and without *RDBP* knockout from GEO (GSE19940) (19). Upon *RDBP* knockdown, 700 genes were differentially expressed (q-value<0.05 and Log2-fold>|1.0|). Among these, many genes were downregulated, such as *PDZK1* (PDZ domain containing 1), *RERG* (Ras-like, estrogen-regulated, growth-inhibitor), *GPX3* (glutathione peroxidase 3), *TIMP1* (Tissue inhibitor of metalloproteinase 1), and *CDKN2C* (Cyclin-dependent kinase 4 inhibitor C). We also observed a mild, but significant induction of *JUNB* upon *RDBP* knockout in the T47D data.

Using available gene expression data, we observed decreased expression of *PDZK1*, *RERG*, and *GPX3* in metastatic PPGL. Unfortunately, we could not evaluate *RDBP* expression in this dataset, as it was not represented.

DISCUSSION

DNA methylation is involved in long-term gene expression programming of cell-type identity and thus, provides a novel reservoir for prognostic markers. Methylation patterns have already proven valuable as prognostic markers in other neoplasms, such as colon and breast cancers. Therefore, it is reasonable to consider that metastatic PPGLs might have unique profiles of DNA methylation that may differentiate them from those without metastasis and also might predict clinical outcome. Early attempts to uncover epigenetic prognostic markers in PPGL generally focused on TSGs hypermethylation (10, 11). Currently, genomic DNA methylation patterns can be interrogated using high-throughput technologies. In fact, global hypermethylation was recently described in *SDHx*-related PPGLs caused by Krebs cycle dysfunction (2, 8). However, these data still are limited and their prognostic value is unclear.

In the present work, whole-genome DNA methylation profiles were obtained using the 27K platform (Illumina). Although the newer 450K platform has replaced the 27K platform, evidences indicate that in terms of general performance both produce consistent and comparable results as previously demonstrated (2). Our results verified that PPGL methylation patterns are strongly influenced by genetic background, exemplified by hierarchical cluster analysis showing two clusters: a "pseudohypoxic" cluster (*VHL*, *SDHx*, and *EPAS1*) and the other containing classical "cluster 2" (*RET*, *NF1*, *TMEM127*, and *MAX*) PPGLs. In addition, unsupervised analysis of DNA methylation profiles proved capable of differentiating *SDHx*-related PPGLs from *VHL*/*EPAS1*- and *RET*/*NF1*/*MAX*-associated tumors. However, hierarchical cluster analysis of DNA methylation profiles was unable to further resolve cluster 2 samples. The two *HRAS*-related tumors were grouped along with cluster 2 tumors. This was not surprising as *HRAS*-related and other cluster 2 tumors (*RET*, *NF1*, *TMEM127*, and *MAX*) converge on a common molecular mechanism characterized by activated MAPK signaling.

DNA methylation differed significantly among PPGL groups ($p<0.0001$). *SDHB*-related tumors showed highest levels of DNA methylation, while *RET*-, *NF1*-, *TMEM127*-, and *MAX*-related PPGLs showed the lowest levels. *VHL*- and *EPAS1*-related tumors had intermediate levels of global DNA methylation with slightly higher levels in *EPAS1*-associated PPGLs. Our results showed the vast majority of CpGs in *SDHB*-related PPGLs were hypermethylated, and verifies previous reports suggesting high-CIMP (2, 8). A wide variety of human neoplasms have been described with high-CIMP (21-23). Prognosis associated with high-CIMP is cell type depend. In glioblastoma and pediatric T-cell acute

lymphoblastic leukemia, high-CIMP is associated with a more favorable prognosis, while poor prognosis has been reported for neuroblastoma and PPGL (2, 21-23). *SDHx* PPGLs, particularly *SDHB*-related have a higher risk to develop metastatic disease (24). Recently, *FH* mutations were described in association with high risk of metastatic disease (25). The Letouzé *et al.* study included 14 metastatic specimens of which one had an *FH* mutation and six had *SDHB* mutations. Severe derangement of metabolic homeostasis cause by mutations in *FH*, *SDHx,* and isocitrate dehydrogenase genes lead to global hypermethylation due to inhibition of alpha-ketoglutarate-dependent dioxygenases, including histone demethylases and TET 5-methylcytosine dioxygenases (2, 8, 26). However, it is likely that the reported association between poor prognosis and high-CIMP in PPGLs are linked to *SDHB* and *FH* mutations, as these are themselves associated with worse outcome. Our hierarchical cluster analysis, showing metastatic PPGLs distributed throughout the dendrogram, provided further evidence indicating that global hypermethylation, while undoubtedly relevant, is not necessarily sufficient to give rise to metastasis.

Supervised analyses comparing *VHL-*, *RET-*, *NF1-*, and *MAX-* with *SDHB*-related tumors revealed specific DNA methylation patterns. We observed hypermethylation of putative TSGs in *SDHB*-related tumors, consistent with high-CIMP in other tumors (9). Also, many pathways potentially affected by DNA methylation in these tumors have important roles in tumorigenesis, such as "pathways in cancer", "MAPK signaling pathway", and "p53 signaling pathways". It is well-known that p53 is essential for cellular responses to DNA damage, and in the great majority of human neoplasms, the p53-network is disrupted (27). It is tempting to speculate that hypermethylation of these TSGs in *SDHB*-related tumors could prevent induction of apoptosis by severe mitochondrial dysfunction caused by *SDHx* deficiency.

Differential methylation of *PNMT* was of particular interest due to its role as a marker of chromaffin cell differentiation and in steroid-induced catecholamine biosynthesis (28). Our results verified *PNMT* hypermethylation previously reported in *SDHB*-related PPGLs (2). PNMT hypomethylation in *RET*- and *NF1*-, and hemimethylation in *VHL*-related PPGLs is highly consistent their associated neurochemical phenotypes (2, 20, 29). However, this model does not explain why other "cluster 1" tumors do not display an adrenergic phenotype, even when *PNMT* is hemimethylated. Also, this does not explain why *MAX*-associated tumors, showing *PNMT* hypomethylation comparable to *RET* and *NF1* tumors, do not display a predominantly adrenergic phenotype. In this context, Qin and colleagues (2014) provided evidence that addressed these paradoxes in other "cluster 1" tumors

characterized by both *EPAS1* expression and stabilization of HIF protein (20). In that study, the authors showed that EPAS1 completely blocked effects of steroid-induced *PNMT* expression in PC12 cells (29). Altogether this provides a rational explaining why all "cluster 1" adrenal pheochromocytomas, including those without a high-CIMP phenotype (e.g., *VHL* and *EPAS1*), do not produce significant epinephrine, as well as the unexpected noradrenergic phenotype presented by *MAX* tumors.

Hypermethylation of *MEG3* was observed in *MAX*-related PPGLs. *MEG3* is a non-coding TSG located on chromosome 14q32 that has been shown to interact with p53 (30). Down-regulation of *MEG3* in *MAX*-related PPGLs has been previously reported (14), and here we provide further evidence indicating *MEG3* down-regulation is caused by aberrant hypermethylation due to a uniparental (paternal) disomy or partial or entire chromosome 14 deletions.

Although not selected for validation by pyrosequencing, it merits mention that other CpGs associated with metastasic PPGL were not only identified in the DS, but also replicated in VS1. In addition, none were contained in the *SDHB*-related list (2), which suggested these CpGs are indeed associated with metastatic PPGLs and not genetic background. Not to mention, many also showed a significant association with TTP even after adjusting for *SDHB* mutation.

For instance, *HDAC11* expression has been described to correlate inversely with proliferative status in non-transformed fibroblasts (31). Also among other candidate CpGs, hypermethylation of the *RASSF1* promoter has been previously described in association with metastatic PPGL and neuroblastoma (2, 10, 11). The probe described by Letouzé et al. differed from the one identified in the present study, as these CpGs mapped to different genomic loci, explaining why it was not removed when we filtered for *SDHB*-associated CpGs (2).

Bioinformatics analyses indicated these CpGs could be involved in nervous system development and regulation of transcription at RNA polymerase II promoters. Initially described as an oncogene, *NTRK1* is primarily expressed in sensory and sympathetic neurons and considered a critical receptor promoting neuronal survival in the presence of NGF. However, recent evidences indicate that NTRK1 acts as a "dependence receptor," as expression of NTRK1 by itself was described to cause neuronal cell death and this activity was prevented by addition of NGF (32, 33). It is widely accepted that PPGL arise through a common mechanism that impedes apoptosis of sympathoadrenal precursors when NGF becomes limiting, which involves NTRK1 (34). Also with roles in nervous system

development, *CYFIP2* is a p53-inducible gene that leads to caspase activation and apoptosis (35, 36). Similarly, CYFIP2 has been shown to negatively modulate survival of colon cancer cells (37). Epigenetic inactivation of *SPOCK2* gene is involved in malignant transformation of ovarian endometriosis (38, 39). Interestingly, *PYGO1* and *BCL9L*, hypermethylated in metastatic PPGL, participate in the nuclear beta-catenin/TCF complex. Composition of beta-catenin/TCF complex transactivators, like BCL9L, PYGO1, and PYGO2, mediate its activity and target specificity to elicit fundamental patterning processes, involving reciprocal epithelial-mesenchymal interactions during tumorigenesis and normal development (e.g. nervous system) (40). The inverse relationship between proliferation and differentiation is well known, and intimately involved in PPGL development. Thus, collective disruption of these factors by aberrant methylation may contribute to PPGL metastases by impairing numerous aspects of nervous system development, such as migration, cellular identity, and differentiation.

Interestingly, we observed aberrant methylation of numerous transcriptional regulators in metastatic PPGLs. In fact, *RDBP* hypermethylation in metastatic PPGLs was highly significant (P=0.003) as shown by pyrosequencing, which indicated its potential diagnostic utility in the clinical setting. The *RDBP* encodes subunit E of the NELF complex, which mediates transcriptional pausing by cooperative binding to elongating RNAPII (41, 42). Transcriptional pausing represents an important regulatory mechanism for many genes, including JUNB (43). Recognized as a key player in neuronal apoptosis as a C-JUN antagonist, depletion of *RDBP* by RNAi was described to enhance *JUNB* expression in human hepatoma cells (34, 43). Data from T47D cells upon *RDBP* silencing helped us identify potential RDBP targets (*JUNB*, *TIMP1*, and *CDKN2C*). Besides its involvement in neuronal apoptosis, JUNB has also been reported to increase the invasive and angiogenic potential in numerous tumors, such as renal cell carcinoma, by inducing *MMP-2/9* (44). *RDBP* knockout decreased the expression of *TIMP1*, which was shown to suppress invasion and metastasis in various human tumors through inhibition of MMP-2/9 (45). Another RDBP target gene identified in the T47D data, *CDKN2C* has been described as a tumor suppressor involved in PPGL and medullary thyroid carcinoma (46).

Although it was not possible to integrate the gene expression and DNA methylation data due to the low numbers of metastatic PPGLs common in both datasets, we were able to observe downregulation of three genes (*PDZK1*, *RERG*, and *GPX3*) both in the T47D data after RDBP KO and metastatic PPGL. This suggests that expression of these three genes may also represent potential markers for metastatic PPGLs. *GPX3* silencing has been reported in metastatic tumors, such as in gastric carcinomas, where it increased migration

and impaired mechanisms regulating reactive oxygen species (47). RERG was reported as a prognostic marker in breast cancer, whose expression correlated inversely proliferation, patient survival, and development of distant metastases (48). It has been reported that PDZK1 forms a complex linking somatostatin receptors and phospholipase C-β (PLC-β), necessary for somatostatin- physiologic responses (49). Although further studies are warranted, epigenetic silencing of *RDBP* in metastatic PPGL may cause global changes in chromatin and/or gene transcription, possibly affecting expression of genes (e.g. *JUNB*, *PDZK1*, *RERG*, *GPX3*) involved with response to apoptotic stimuli and invasion, proliferation, and metabolism.

In conclusion, this is the first high-throughput study to explore DNA methylation in metastatic PPGL, as well as PPGLs with diverse genetic backgrounds. We demonstrate that DNA methylation patterns differ according to PPGL genotype, and verify *SDHx*-related tumors display high-CIMP. Also, our results indicate that metastatic PPGLs are not necessarily associated with the high-CIMP previously described in relation to *SDHx*/*FH* mutations (2, 8). Most importantly, we identified and validated 52 CpGs associated with the development of metastases in two large independent cohorts of these rare tumors. Aberrant methylation of these CpGs could make metastatic PPGLs less sensitive to proapoptotic stimuli and warrants further investigation. Of these, forty-eight CpGs showed significant associations with TTP. Our bioinformatics analyses and previous experimental evidences suggest aberrant DNA methylation metastatic PPGLs could affect nervous system development and transcriptional regulation. Finally, *RDBP* hypermethylation was further confirmed in metastatic PPGL by pyrosequencing in an independent series and should be assessed as a new prognostic marker for metastatic PPGL.

REFERENCES

1. Dahia PL. Pheochromocytoma and paraganglioma pathogenesis: learning from genetic heterogeneity. Nature reviews Cancer. 2014;14:108-19.
2. Letouze E, Martinelli C, Loriot C, Burnichon N, Abermil N, Ottolenghi C, et al. SDH mutations establish a hypermethylator phenotype in paraganglioma. Cancer cell. 2013;23:739-52.
3. Lopez-Jimenez E, Gomez-Lopez G, Leandro-Garcia LJ, Munoz I, Schiavi F, Montero-Conde C, et al. Research resource: Transcriptional profiling reveals different pseudohypoxic signatures in SDHB and VHL-related pheochromocytomas. Molecular endocrinology. 2010;24:2382-91.
4. de Cubas AA, Leandro-Garcia LJ, Schiavi F, Mancikova V, Comino-Mendez I, Inglada-Perez L, et al. Integrative analysis of miRNA and mRNA expression profiles in pheochromocytoma and paraganglioma identifies genotype-specific markers and potentially regulated pathways. Endocrine-related cancer. 2013;20:477-93.
5. Martiniova L, Lu J, Chiang J, Bernardo M, Lonser R, Zhuang Z, et al. Pharmacologic modulation of serine/threonine phosphorylation highly sensitizes PHEO in a MPC cell and mouse model to conventional chemotherapy. PloS one. 2011;6:e14678.
6. Lv P, Wang Y, Ma J, Wang Z, Li JL, Hong CS, et al. Inhibition of protein phosphatase 2A with a small molecule LB100 radiosensitizes nasopharyngeal carcinoma xenografts by inducing mitotic catastrophe and blocking DNA damage repair. Oncotarget. 2014;5:7512-24.
7. Hadoux J, Favier J, Scoazec JY, Leboulleux S, Al Ghuzlan A, Caramella C, et al. SDHB mutations are associated with response to temozolomide in patients with metastatic pheochromocytoma or paraganglioma. International journal of cancer Journal international du cancer. 2014;135:2711-20.
8. Killian JK, Kim SY, Miettinen M, Smith C, Merino M, Tsokos M, et al. Succinate dehydrogenase mutation underlies global epigenomic divergence in gastrointestinal stromal tumor. Cancer discovery. 2013;3:648-57.
9. Jones PA, Baylin SB. The fundamental role of epigenetic events in cancer. Nature reviews Genetics. 2002;3:415-28.
10. Astuti D, Agathanggelou A, Honorio S, Dallol A, Martinsson T, Kogner P, et al. RASSF1A promoter region CpG island hypermethylation in phaeochromocytomas and neuroblastoma tumours. Oncogene. 2001;20:7573-7.
11. Geli J, Kiss N, Lanner F, Foukakis T, Natalishvili N, Larsson O, et al. The Ras effectors NORE1A and RASSF1A are frequently inactivated in pheochromocytoma and abdominal paraganglioma. Endocrine-related cancer. 2007;14:125-34.
12. Altman DG, McShane LM, Sauerbrei W, Taube SE. Reporting Recommendations for Tumor Marker Prognostic Studies (REMARK): explanation and elaboration. PLoS medicine. 2012;9:e1001216.
13. Comino-Mendez I, de Cubas AA, Bernal C, Alvarez-Escola C, Sanchez-Malo C, Ramirez-Tortosa CL, et al. Tumoral EPAS1 (HIF2A) mutations explain sporadic pheochromocytoma and paraganglioma in the absence of erythrocytosis. Human molecular genetics. 2013;22:2169-76.
14. Comino-Mendez I, Gracia-Aznarez FJ, Schiavi F, Landa I, Leandro-Garcia LJ, Leton R, et al. Exome sequencing identifies MAX mutations as a cause of hereditary pheochromocytoma. Nature genetics. 2011;43:663-7.

15. Bibikova M, Le J, Barnes B, Saedinia-Melnyk S, Zhou L, Shen R, et al. Genome-wide DNA methylation profiling using Infinium(R) assay. Epigenomics. 2009;1:177-200.
16. Du P, Zhang X, Huang CC, Jafari N, Kibbe WA, Hou L, et al. Comparison of Beta-value and M-value methods for quantifying methylation levels by microarray analysis. BMC bioinformatics. 2010;11:587.
17. Wilkerson MD, Hayes DN. ConsensusClusterPlus: a class discovery tool with confidence assessments and item tracking. Bioinformatics. 2010;26:1572-3.
18. Gentleman RC, Carey VJ, Bates DM, Bolstad B, Dettling M, Dudoit S, et al. Bioconductor: open software development for computational biology and bioinformatics. Genome biology. 2004;5:R80.
19. Sun J, Li R. Human negative elongation factor activates transcription and regulates alternative transcription initiation. The Journal of biological chemistry. 2010;285:6443-52.
20. Qin N, de Cubas AA, Garcia-Martin R, Richter S, Peitzsch M, Menschikowski M, et al. Opposing effects of HIF1alpha and HIF2alpha on chromaffin cell phenotypic features and tumor cell proliferation: Insights from MYC-associated factor X. International journal of cancer Journal international du cancer. 2014;135:2054-64.
21. Borssen M, Palmqvist L, Karrman K, Abrahamsson J, Behrendtz M, Heldrup J, et al. Promoter DNA methylation pattern identifies prognostic subgroups in childhood T-cell acute lymphoblastic leukemia. PloS one. 2013;8:e65373.
22. Abe M, Ohira M, Kaneda A, Yagi Y, Yamamoto S, Kitano Y, et al. CpG island methylator phenotype is a strong determinant of poor prognosis in neuroblastomas. Cancer research. 2005;65:828-34.
23. Noushmehr H, Weisenberger DJ, Diefes K, Phillips HS, Pujara K, Berman BP, et al. Identification of a CpG island methylator phenotype that defines a distinct subgroup of glioma. Cancer cell. 2010;17:510-22.
24. Amar L, Baudin E, Burnichon N, Peyrard S, Silvera S, Bertherat J, et al. Succinate dehydrogenase B gene mutations predict survival in patients with malignant pheochromocytomas or paragangliomas. The Journal of clinical endocrinology and metabolism. 2007;92:3822-8.
25. Castro-Vega LJ, Buffet A, De Cubas AA, Cascon A, Menara M, Khalifa E, et al. Germline mutations in FH confer predisposition to malignant pheochromocytomas and paragangliomas. Human molecular genetics. 2014;23:2440-6.
26. Xu W, Yang H, Liu Y, Yang Y, Wang P, Kim SH, et al. Oncometabolite 2-hydroxyglutarate is a competitive inhibitor of alpha-ketoglutarate-dependent dioxygenases. Cancer cell. 2011;19:17-30.
27. Tobiume K. Involvement of Bcl-2 family proteins in p53-induced apoptosis. Journal of Nippon Medical School = Nippon Ika Daigaku zasshi. 2005;72:192-3.
28. Anderson DJ, Michelsohn A. Role of glucocorticoids in the chromaffin-neuron developmental decision. International journal of developmental neuroscience : the official journal of the International Society for Developmental Neuroscience. 1989;7:475-87.
29. Huynh TT, Pacak K, Wong DL, Linehan WM, Goldstein DS, Elkahloun AG, et al. Transcriptional regulation of phenylethanolamine N-methyltransferase in pheochromocytomas from patients with von Hippel-Lindau syndrome and multiple endocrine neoplasia type 2. Annals of the New York Academy of Sciences. 2006;1073:241-52.

30. Lu KH, Li W, Liu XH, Sun M, Zhang ML, Wu WQ, et al. Long non-coding RNA MEG3 inhibits NSCLC cells proliferation and induces apoptosis by affecting p53 expression. BMC cancer. 2013;13:461.
31. Bagui TK, Sharma SS, Ma L, Pledger WJ. Proliferative status regulates HDAC11 mRNA abundance in nontransformed fibroblasts. Cell cycle. 2013;12:3433-41.
32. Nikoletopoulou V, Lickert H, Frade JM, Rencurel C, Giallonardo P, Zhang L, et al. Neurotrophin receptors TrkA and TrkC cause neuronal death whereas TrkB does not. Nature. 2010;467:59-63.
33. Bredesen DE, Mehlen P, Rabizadeh S. Receptors that mediate cellular dependence. Cell death and differentiation. 2005;12:1031-43.
34. Lee S, Nakamura E, Yang H, Wei W, Linggi MS, Sajan MP, et al. Neuronal apoptosis linked to EglN3 prolyl hydroxylase and familial pheochromocytoma genes: developmental culling and cancer. Cancer cell. 2005;8:155-67.
35. Jackson RS, 2nd, Cho YJ, Stein S, Liang P. CYFIP2, a direct p53 target, is leptomycin-B sensitive. Cell cycle. 2007;6:95-103.
36. Pittman AJ, Gaynes JA, Chien CB. nev (cyfip2) is required for retinal lamination and axon guidance in the zebrafish retinotectal system. Developmental biology. 2010;344:784-94.
37. Mongroo PS, Noubissi FK, Cuatrecasas M, Kalabis J, King CE, Johnstone CN, et al. IMP-1 displays cross-talk with K-Ras and modulates colon cancer cell survival through the novel proapoptotic protein CYFIP2. Cancer research. 2011;71:2172-82.
38. Ren F, Wang DB, Li T. [Epigenetic inactivation of SPOCK2 in the malignant transformation of ovarian endometriosis]. Zhonghua fu chan ke za zhi. 2011;46:822-5.
39. Schnepp A, Komp Lindgren P, Hulsmann H, Kroger S, Paulsson M, Hartmann U. Mouse testican-2. Expression, glycosylation, and effects on neurite outgrowth. The Journal of biological chemistry. 2005;280:11274-80.
40. Kramps T, Peter O, Brunner E, Nellen D, Froesch B, Chatterjee S, et al. Wnt/wingless signaling requires BCL9/legless-mediated recruitment of pygopus to the nuclear beta-catenin-TCF complex. Cell. 2002;109:47-60.
41. Yamaguchi Y, Takagi T, Wada T, Yano K, Furuya A, Sugimoto S, et al. NELF, a multisubunit complex containing RD, cooperates with DSIF to repress RNA polymerase II elongation. Cell. 1999;97:41-51.
42. Yamaguchi Y, Inukai N, Narita T, Wada T, Handa H. Evidence that negative elongation factor represses transcription elongation through binding to a DRB sensitivity-inducing factor/RNA polymerase II complex and RNA. Molecular and cellular biology. 2002;22:2918-27.
43. Aida M, Chen Y, Nakajima K, Yamaguchi Y, Wada T, Handa H. Transcriptional pausing caused by NELF plays a dual role in regulating immediate-early expression of the junB gene. Molecular and cellular biology. 2006;26:6094-104.
44. Kanno T, Kamba T, Yamasaki T, Shibasaki N, Saito R, Terada N, et al. JunB promotes cell invasion and angiogenesis in VHL-defective renal cell carcinoma. Oncogene. 2012;31:3098-110.
45. Stamenkovic I. Matrix metalloproteinases in tumor invasion and metastasis. Seminars in cancer biology. 2000;10:415-33.
46. van Veelen W, Klompmaker R, Gloerich M, van Gasteren CJ, Kalkhoven E, Berger R, et al. P18 is a tumor suppressor gene involved in human medullary

thyroid carcinoma and pheochromocytoma development. International journal of cancer Journal international du cancer. 2009;124:339-45.
47. Peng DF, Hu TL, Schneider BG, Chen Z, Xu ZK, El-Rifai W. Silencing of glutathione peroxidase 3 through DNA hypermethylation is associated with lymph node metastasis in gastric carcinomas. PloS one. 2012;7:e46214.
48. Habashy HO, Powe DG, Glaab E, Ball G, Spiteri I, Krasnogor N, et al. RERG (Ras-like, oestrogen-regulated, growth-inhibitor) expression in breast cancer: a marker of ER-positive luminal-like subtype. Breast cancer research and treatment. 2011;128:315-26.
49. Kim JK, Kwon O, Kim J, Kim EK, Park HK, Lee JE, et al. PDZ domain-containing 1 (PDZK1) protein regulates phospholipase C-beta3 (PLC-beta3)-specific activation of somatostatin by forming a ternary complex with PLC-beta3 and somatostatin receptors. The Journal of biological chemistry. 2012;287:21012-24.

TABLE AND FIGURE LEGENDS

Table 1. Clinical summary for PPGL samples.

a) Total samples. b) Tumors without metastases. c) Tumors with metastases. Tumors were considered metastatic when patients presented metastasis in sites normally devoid of chromaffin tissue (e.g. lung, liver, bone, lymph nodes), either synchronous or metachronous. Diagnosis of metastasis was based on imaging evidence or pathological confirmation. d) Normal adrenal medulla (not included in analysis).

Table 2. Differentially methylated CpGs for PPGL experimental group comparisons.

a) CpGs initially identified in Discovery Series. b) CpG successfully replicated in Validation Series 1. c) Hypermethylated CpGs. d) Hypomethylated CpGs. d) Not available due to lack of *EPAS1* samples in Validation Series 1.

Table 3. CpGs associated with metastatic PPGL.

a) Illumina 27k probe ID. b) $\Delta\beta = \beta_{metastatic}-\beta_{Benign}$. c) %M: Percent metastatic tumors with alteration. d) q-val: adjusted p-value for multiple testing. e) q-value corrected for *SDHB* mutation status and series origin.

Figure 1. DNA methylation patterns in PPGL.

A and B) Unsupervised cluster analyses of PPGL samples based on their DNA methylation patterns. The top 500 probes with the highest variance across all samples were used for unsupervised analyses. A) Hierarchical cluster analysis. Distance was calculated by Pearson's correlation method and CpGs were clustered by complete linkage clustering method. Heatmap was shown for top 10 CpGs. Hypermethylated CpGs are shown in red, whereas hypomethylated CpGs are indicated in blue. "M" or "B" prefix in from of sample names indicates "metastatic" or "benign," respectively. Cluster C1A (indicated by pale red highlight) represented hypermethylator group, containing *SDHx* tumors. Cluster C1B (indicated by green highlight) contained *VHL* and *EPAS1* tumors, with intermediate methylation. Cluster C2 (indicated by light blue highlight) had samples with lowest levels of global methylation and contained *RET*, *NF1*, *TMEM127*, *MAX*, and *HRAS* tumors. B) K-means clustering of DNA methylation profiles. Optimal classification defined three clusters. C) Circos plot of CpG methylation levels for PPGL genetic groups. From outside to in, first track provides chromosome cytobands, followed by heatmaps showing DNA methylation for PPGL genetic groups with mutations in *SDHB* (second track), *VHL* (third

track), *EPAS1* (forth track), *RET* (fifth track), *NF1* (sixth track), and *MAX* (seventh track). Well-known tumor suppressor genes (TSGs) are indicated by purple dots. Genes with functions in apoptotic signaling are indicated by red dots. Genes involved with WNT signaling are indicated with yellow dots. Green dots indicate genes involved in catecholamine biosynthesis and secretion. Heatmap legend in center: DNA methylation shown as β-values with hypermethylation in red ($0<\beta<0.5$) and hypomethylation in blue ($0.5<\beta<1$). D) Global DNA methylation levels for each PPGL group. Global DNA methylation represented as β-values ($0<\beta<0.5$: Hypomethylated; $0.5<\beta<1$: hypermethylated). E) Group-specific CpGs. Venn diagram analysis performed with only those CpGs that had been replicated in VS1. All comparisons were performed relative to *SDHB* tumors. Thus, the 361 "hypomethylated" CpGs indicated in the *SDHB* box (red) means that these CpGs were hypomethylated relative to the other experimental groups. Therefore, these 361 CpGs were actually hypermethylated in *SDHB*.

Figure 2. DNA methylation patterns associated with metastatic CpGs.

A) Circos plot showing 52 validated. Outermost track provides ideogram for all chromosomes, except chromosomes 14, 18, 21, 22, X, and Y. Heatmaps show methylation levels for 52 confirmed CpGs associated with metastatic PPGL a) Metastatic tumors in DS; b) Tumors without metastases in DS; c) Metastatic tumors in VS1; d) Tumors without metastases in VS1. Green dots indicate gene with functions in nervous system development, while genes involved with transcriptional regulation at gene promoters are indicated by orange dots. Hypermethylated CpGs are indicated in red, whereas hypomethylated CpGs are indicated in blue. B-D) Kaplan-Meier survival curves for select CpGs associated with worse TTP (n=233, 23 events). Red line indicates hypermethylated tumors and blue line represents hypomethylated tumors. The HR and associated q-value (p-value adjusted for SDHB status and series, and multiple testing) represented were considering methylation levels as continuous variables. B) RDBP_cg06351503: HR 3.0(CI95%, 2.0-4.4); q-value=0.001. Log rank test p-value=$6.3\text{x}10^{-5}$. Hypermethylated (n=117; 21 events), Hypomethylated (n=116; 2 events); median methylation: M=-0.93, β=0.34. C) HDAC11_cg05446471: HR 1.5(CI95%, 1.1-2.0); q-value=0.047. Log rank test p-value=0.007. Hypermethylated (n=118; 20 events), Hypomethylated (n=115; 3 events); median methylation: M=-0.29, β=0.45. D) CYFIP2_cg00986320: HR 2.0(CI95%, 1.3-2.9); q-value=0.006. Log rank test p-value=0.002. Hypermethylated (n=118; 20 events), Hypomethylated (n=115; 3 events); median methylation: M=0.77, β=0.63.

A. Hierarchial cluster analysis

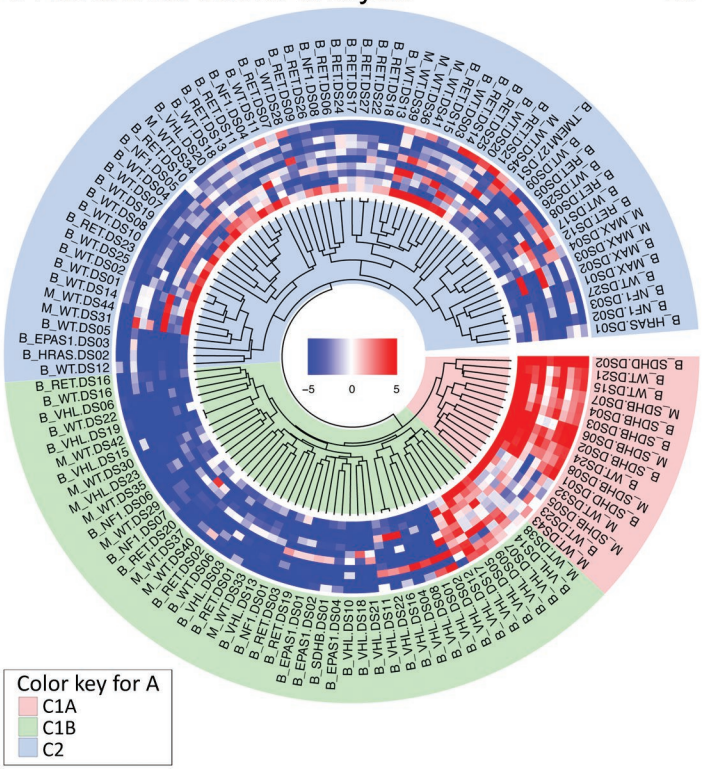

B. Consensus cluster analysis

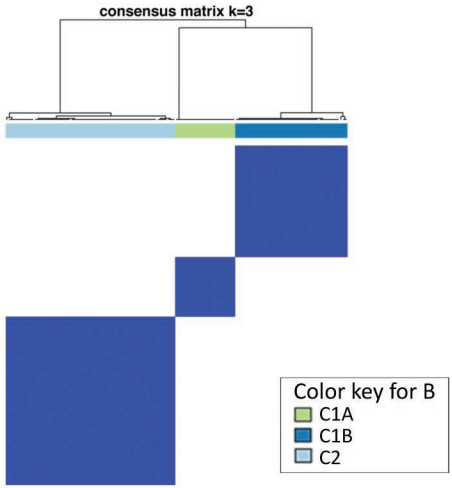

D. Global methylation levels for PPGL genetic groups

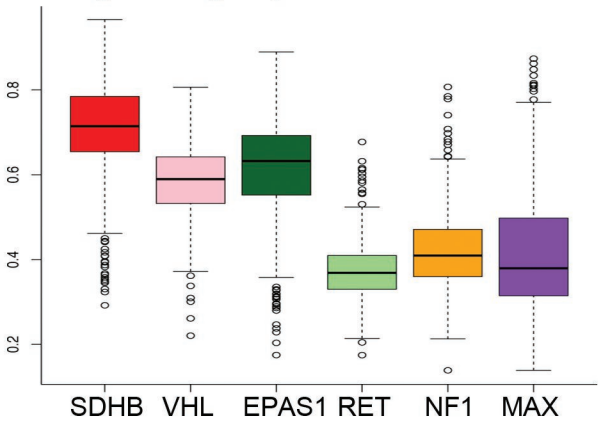

C. Global view of CpG methylation levels

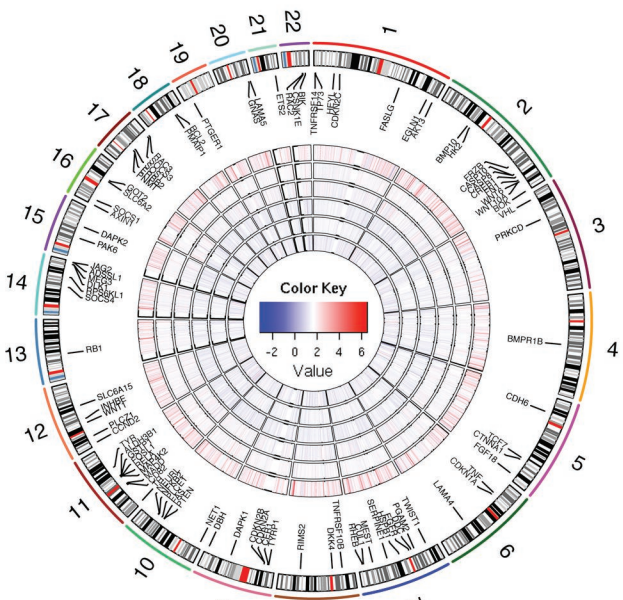

E. Venn diagram for genotype specific CpGs

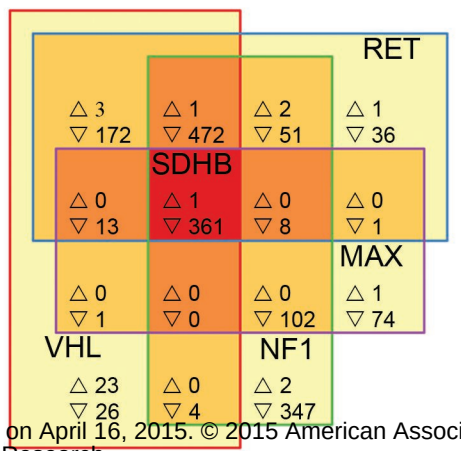

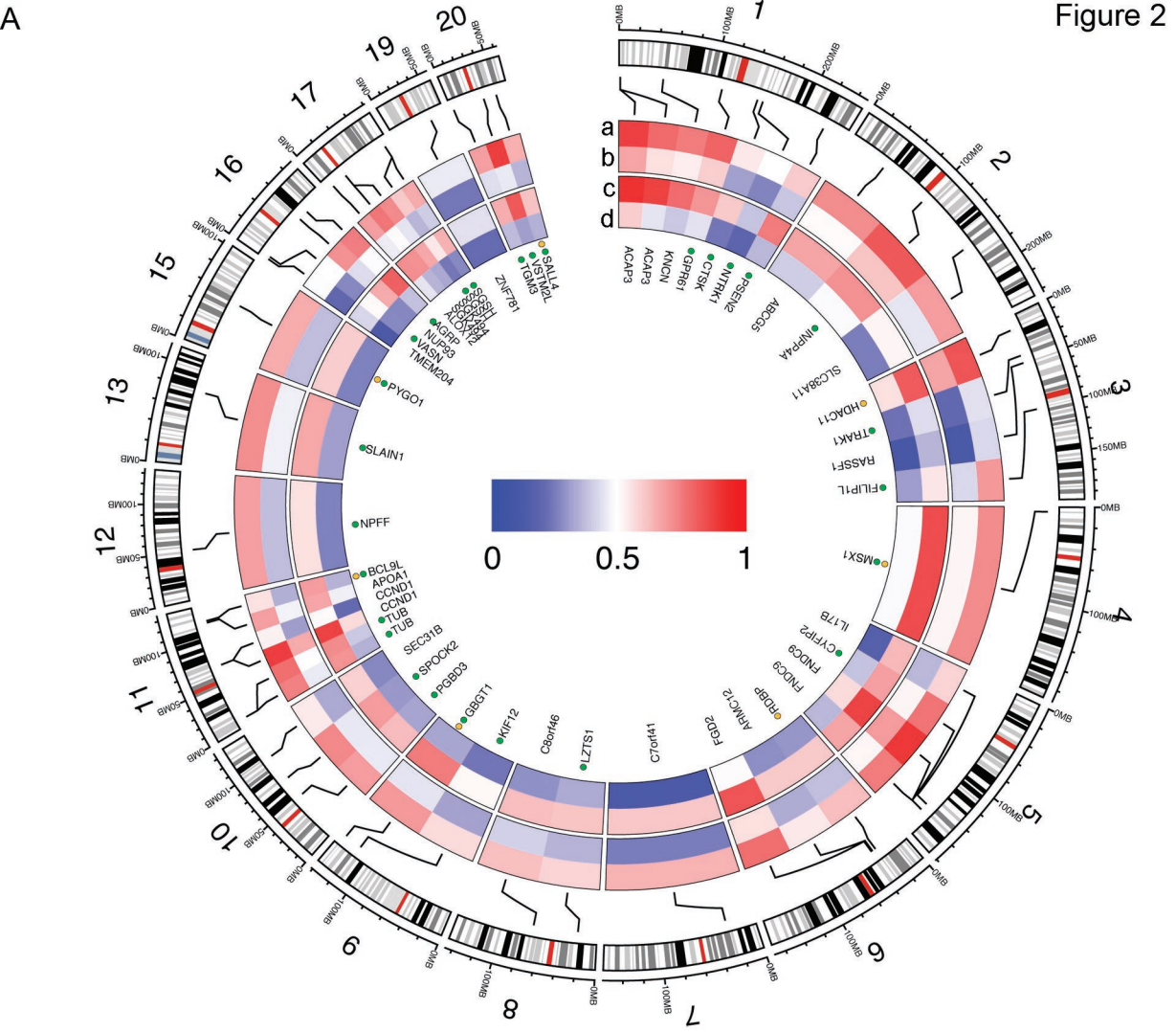

Table 1. Clinical summary for methylation study tumors

	Discovery Series			Validation Series 1			Validation Series 2		
	N[a]	Ben[b]	Met[c]	*N*[a]	Ben[b]	Met[c]	*N*[a]	Ben[b]	Met[c]
VHL	23	22	1	24	19	5	3	2	1
RET	26	26	-	13	13	-	-	-	-
NF1	8	8	-	30	28	2	-	-	-
SDHA	-	-	-	1	1	-	1	-	1
SDHB	8	4	4	16	6	10	3	3	-
SDHC	-	-	-	1	1	-	-	-	-
SDHD	2	2	-	3	3	-	-	-	-
FH	-	-	-	1	-	1	-	-	-
EPAS1	4	4	-	-	-	-	-	-	-
MAX	4	2	2	4	4	-	-	-	-
HRAS	2	2	-	-	-	-	2	1	1
TMEM127	1	1	-	1	1	-	-	-	-
WT	45	28	17	60	54	6	24	8	16
N[a] PPGL	123	99	24	154	130	24	33	14	19
nAM[d]	-			3			-		

Table 2. Differentially methylated CpGs for PPGL experimental group comparisons

Comparison	CpGs in DS[a]		Replicated in VS1[b]	
	Hyper[c]	Hypo[d]	Hyper[c]	Hypo[d]
VHL vs. *SDHB*	143	1265	28	1049
EPAS1 vs. *SDHB*	4	172	N/A[d]	N/A[d]
RET vs. *SDHB*	145	1266	8	1114
NF1 vs. *SDHB*	12	1476	6	1345
MAX vs. *SDHB*	8	782	2	560

Table 3. Confirmed CpGs associated with PPGL malignancy

Probe ID[a]	Gene	Discovery Series			Validation Series 1			Cox Regression	
		Δβ[b]	%M[c]	q-val[d]	Δβ[b]	%M[c]	q-val[d]	HR(95%CI)	q-val[d,e]
cg2578116	ABCG5	0.2	62.5	0.0447	0.2	66.7	4.2E-05	1.6 (1.2-2.2)	0.016
cg2520398	ACAP3	0.2	75.0	0.0125	0.4	70.8	8.1E-08	1.6 (1.2-2.3)	0.013
cg1856551	ACAP3	0.2	79.2	0.0230	0.3	75.0	3.1E-08	1.5 (1.1-2.2)	0.077
cg0681046	AGRP	0.2	70.8	0.0185	0.4	83.3	1.0E-06	2.1 (1.4-3.0)	0.001
cg0894633	ALOX12	0.2	66.7	0.0203	0.2	50.0	0.00024	1.5 (1.0-2.1)	0.052
cg1932462	APOA1	0.2	62.5	0.0403	0.2	62.5	0.00787	1.7 (1.1-2.6)	0.138
cg2599472	ARMC1	0.2	50.0	0.0830	0.3	50.0	2.0E-05	2.3 (1.5-3.5)	0.013
cg2002920	BCL9L	0.2	62.5	0.0417	0.3	54.2	2.2E-06	1.6 (1.1-2.2)	0.032
cg0897217	C7orf41	0.3	54.2	0.0060	0.4	54.2	1.5E-07	1.8 (1.4-2.4)	0.007
cg2370436	C8orf46	0.2	50.0	0.0084	0.3	62.5	3.3E-07	2.2 (1.5-3.2)	0.010
cg0742696	CCND1	0.2	83.3	0.0094	0.3	83.3	6.6E-06	2.1 (1.4-3.4)	0.026
cg1360809	CCND1	0.2	58.3	0.0125	0.3	83.3	3.3E-05	1.6 (1.2-2.1)	0.013
cg2080239	CTSK	0.2	62.5	0.0230	0.3	62.5	4.7E-07	2.2 (1.4-3.2)	0.002
cg0098632	CYFIP2	0.2	66.7	0.0590	0.3	66.7	1.4E-05	2.0 (1.3-2.9)	0.006
cg0022692	FGD2	0.2	79.2	0.0438	0.3	79.2	0.00012	1.6 (1.1-2.1)	0.017
cg0643650	FILIP1L	0.2	75.0	0.0002	0.2	50.0	1.0E-06	2.7 (1.8-3.9)	0.004
cg2018978	FNDC9	0.2	70.8	0.0070	0.3	62.5	1.2E-06	1.7 (1.2-2.4)	0.013
cg2679005	FNDC9	0.2	70.8	0.036	0.3	87.5	1.0E-06	1.7 (1.2-2.4)	0.013
cg0116977	GBGT1	0.2	58.3	0.0451	0.4	70.8	8.7E-08	1.9 (1.4-2.7)	0.002
cg2374904	GPR61	0.2	75.0	0.0743	0.2	62.5	0.05922	1.2 (0.9-1.7)	0.539
cg0544647	HDAC1	0.2	79.2	0.0439	0.2	75.0	0.00067	1.5 (1.1-2.0)	0.047
cg2514149	IL17B	0.2	58.3	0.0145	0.4	75.0	5.3E-07	1.8 (1.3-2.6)	0.007
cg0116961	INPP4A	0.2	66.7	0.0683	0.2	62.5	0.00114	1.6 (1.1-2.4)	0.137
cg0283849	KIF12	0.2	58.3	0.0029	0.2	79.2	9.8E-07	2.1 (1.5-2.8)	0.002
cg1998721	KNCN	0.2	70.8	0.0552	0.3	79.2	1.7E-05	1.6 (1.2-2.2)	0.072
cg2691799	LZTS1	0.2	62.5	0.0465	0.2	50.0	8.3E-05	1.8 (1.3-2.7)	0.077
cg0974897	MSX1	0.2	62.5	0.0198	0.3	54.2	1.1E-07	1.5 (1.2-1.9)	0.016
cg0165738	NPFF	0.3	62.5	0.0042	0.2	66.7	8.7E-08	2.0 (1.4-2.9)	0.001
cg0062611	NTRK1	0.2	62.5	0.0009	0.2	54.2	1.1E-05	2.2 (1.4-3.4)	0.023
cg1058675	NUP93	0.2	66.7	0.0392	0.3	62.5	2.3E-06	1.5 (1.1-2.1)	0.029
cg0198259	PGBD3	0.2	66.7	0.0235	0.3	75.0	8.7E-08	2.6 (1.7-4.0)	0.002
cg2551430	PSEN2	0.2	50.0	0.0389	0.3	50.0	4.2E-07	1.7 (1.2-2.4)	0.014
cg2341277	PYGO1	0.2	50.0	0.0234	0.3	62.5	4.0E-08	1.8 (1.2-2.5)	0.004
cg2155455	RASSF	0.3	58.3	0.0160	0.2	50.0	0.00027	1.6 (1.2-2.1)	0.037
cg0635150	RDBP	0.2	50.0	0.0010	0.3	70.8	4.0E-07	3.0 (2.0-4.4)	0.001
cg0630323	SALL4	0.2	50.0	0.0098	0.2	50.0	2.5E-06	1.8 (1.3-2.5)	0.005
cg2670556	SEC31B	0.2	66.7	0.0152	0.3	54.2	5.2E-06	1.8 (1.3-2.7)	0.010
cg0907658	SGK494	0.2	70.8	0.0038	0.3	83.3	6.4E-08	2.5 (1.7-3.6)	0.001
cg2268652	SGK494	0.2	83.3	0.0103	0.3	79.2	2.7E-07	2.6 (1.6-4.4)	0.006
cg0767568	SGSH	0.2	66.7	0.0011	0.3	66.7	8.2E-07	2.4 (1.7-3.6)	0.002
cg0514073	SGSH	0.2	75.0	0.0014	0.3	54.2	7.5E-07	1.9 (1.4-2.5)	0.006
cg1978259	SLAIN1	0.2	62.5	0.0493	0.3	70.8	6.1E-07	2.6 (1.6-4.0)	0.006
cg0414380	SLC38A	0.2	75.0	0.0015	0.2	54.2	1.6E-05	2.6 (1.6-4.0)	0.009
cg0186150	SPOCK	0.2	83.3	0.0189	0.3	70.8	4.6E-05	1.7 (1.2-2.3)	0.014
cg2161170	TGM3	0.2	66.7	0.0279	0.2	66.7	0.00135	1.9 (1.3-2.8)	0.057
cg1770617	TMEM2	0.2	70.8	0.0028	0.2	50.0	2.7E-06	1.6 (1.2-2.2)	0.013
cg2487784	TRAK1	0.2	83.3	0.0009	0.2	54.2	6.8E-05	2.4 (1.5-3.8)	0.014
cg1548047	TUB	0.2	70.8	0.0017	0.3	70.8	2.5E-07	2.1 (1.4-3.0)	0.004
cg0549211	TUB	0.2	70.8	0.0029	0.3	79.2	4.9E-07	2.1 (1.4-3.0)	0.009
cg0927645	VASN	0.2	66.7	0.0076	0.2	50.0	0.00034	1.8 (1.1-2.7)	0.269
cg1159950	VSTM2	0.4	58.3	0.0707	0.5	58.3	1.3E-06	1.5 (1.2-1.9)	0.035
cg1071043	ZNF781	0.2	62.5	0.0051	0.2	70.8	0.00011	1.8 (1.3-2.5)	0.037

AACR American Association for Cancer Research

Clinical Cancer Research

DNA methylation profiling in pheochromocytoma and paraganglioma reveals diagnostic and prognostic markers.

Aguirre A de Cubas, Esther Korpershoek, Lucia Inglada-Perez, et al.

Clin Cancer Res Published OnlineFirst March 30, 2015.